Eur. Phys. J. B **51**, 195–208 (2006)
DOI: 10.1140/epjb/e2006-00215-9

THE EUROPEAN PHYSICAL JOURNAL B

Kinetic Monte Carlo and density functional study of hydrogen enhanced dislocation glide in silicon

S. Scarle[1,a] and C.P. Ewels[2,3,b]

[1] Department of Computer Sciences, University of Sheffield, Regent Court, 211 Portobello Road, Sheffield, S1 4DP, UK
[2] Institut des Matériaux Jean Rouxel, CNRS-Université de Nantes, UMR6502, 2 rue de la Houssinière, B.P. 32229, 44322 Nantes, France
[3] Laboratoire de Physiques des Solides, Université Paris Sud, bâtiment 510, 91405 Orsay, France

Received 22 November 2005 / Received in final form 28 February 2006
Published online 2 June 2006 –

Abstract. We investigate Hydrogen Enhanced Dislocation Glide [HEDG], using n-fold way Kinetic Monte Carlo simulations of the interaction between hydrogen and 90° partial dislocations in silicon, and a range of new density functional calculations. We examine two different hydrogen arrival species, as well as hydrogen recombination at the dislocation. The Monte Carlo simulations use a line-wise description of the dislocation line parameterized using density functional calculations of migration and formation energies of various dislocation line defects and their complexes with hydrogen.
From this we suggest that the rate of H_2 expulsion from the dislocation core increases as we approach HEDG, but that if the concentration of the hydrogen species goes beyond that required for HEDG it then slows dislocation motion by choking the line with defects comprised of two hydrogen atoms in a reconstruction bond. A 'dislocation engine' model is proposed whereby hydrogen enters the dislocation line, catalyses motion, and is expelled along the core as H_2.

PACS. 61.72.Hh Indirect evidence of dislocations and other defects (resistivity, slip, creep, strains, internal friction, EPR, NMR, etc.) – 61.72.Bb Theories and models of crystal defects – 61.72.Lk Linear defects: dislocations, disclinations

1 Introduction

The problem of dislocations in semiconductors is coming into the capabilities of modern hybrid computing techniques. These use static first principle calculations of significant processes to parameterize kinetic Monte Carlo models of large scale processes. Following on from our previous work [1,2] on the 90° partial dislocation in silicon, we now present work on Hydrogen Enhanced Dislocation Glide [HEDG] in the same system. We use the same linewise description of the dislocation line in an n-fold way kinetic Monte Carlo [nkMC] simulation, but add further defect structures and many more interactions to introduce hydrogen into the system.

Hydrogen in silicon was originally considered a low concentration impurity whose primary rôle in the passivation of electrically active defects [3,4]. This is partly because hydrogen in silicon is difficult to detect using standard techniques, such as Fourier Transform Infra-Red [FTIR] and Raman Spectroscopy. More recent work suggests silicon wafer samples may contain hydrogen concentrations which equal that of acceptors and largely exceeds that of donors in highly doped materials (impurity concentration $N_i \geq 10^{17}$ cm^{-3}), while it is always greater than the dopant concentration in low doped material ($N_i \leq 10^{15}$ cm^{-3}) [5].

As well as its electronic rôle, hydrogen has become an important silicon dopant for its mechanical properties. Hydrogen has assumed industrial importance in silicon wafer technology through the use of ion implantation techniques, notably the SmartCut^{TM} process [6] used in silicon-on-insulator technology. In this case a dense layer of hydrogen is implanted into silicon and annealed, whereupon fractures form along the implantation plane leaving an atomically smooth surface. In addition implanted hydrogen can form platelets [7].

Work by Yamashita et al. on hydrogen implanted samples showed that hydrogen has a strong effect on dislocation mobility, lowering the activation barrier to motion for dislocations [8] from 2.2 eV to 1.2 eV. These processes (e.g. SmartCut and HEDG) may prove to be closely linked, as the SmartCut process has been shown to have a similar activation energy [9] ∼1.2 eV.

Furthermore, studies of H-plasma-treated dislocated silicon [10] show that dislocations, in common with some point defects [5], act as recombination sites for H atoms

[a] e-mail: s.scarle@sheffield.ac.uk
[b] e-mail: chris@ewels.info

to form H_2 molecules. It is clear from all these effects that hydrogen is able to interact with its silicon host and directly affect its mechanical behaviour. Although recent ab initio results point the way to various atomic scale process for such interactions [11], there has yet to be developed a coherent picture of the atomic scale processes and their interaction, for hydrogen and dislocations in silicon.

In this paper we present results from new ab initio density functional calculations for different interactions between hydrogen and silicon dislocation cores. We then present a number of nkMC simulations of hydrogen effected dislocation motion, using our line-wise description of the dislocation line. The nkMC is parameterized using the new ab initio data presented here and that given in the work of Ewels et al. [11] and Öberg et al. [12]. These simulations allow comparison between two different hydrogen-dislocation line combination scenarios: either atomic hydrogen arriving at the line and forming a silicon bond centred hydrogen atom or as molecular hydrogen under going a similar process. We then study the effectiveness of the dislocation as a site for hydrogen recombination in each case.

From this we acquire evidence to suggest that bond centred atomic hydrogen trapped on the dislocation line may be the main driving defect for HEDG. Also, once a critical concentration of mobile hydrogen has been reached for HEDG, any further increase appears to kill the HEDG effect. Further, there is an increase in hydrogen recombination while HEDG is taking place.

2 Experimental background

The introduction of hydrogen to silicon reduces the activation barrier for dislocation motion from 2.2 eV to 1.2 eV, as well as reducing the prefactor by orders of magnitude [8]. HEDG has this in common with the related radiation enhanced dislocation glide [REDG] [13]. In their work, Yamashita et al. observed the dislocation velocity after a pre-hydrogenation treatment at 500 °C for 1 h, in a temperature range of 390 °C to 480 °C. Without H:

$$\nu_{dis} = 7 \times 10^5 \text{ ms}^{-1} \exp\left(-\frac{2.2 \text{ eV}}{k_B T}\right); \quad (1)$$

with H:

$$\nu_{dis} = 2 \text{ ms}^{-1} \exp\left(-\frac{1.2 \text{ eV}}{k_B T}\right). \quad (2)$$

No enhancement effect was observed above 500 °C. The necessity for the pre-hydrogenation step has lead to the suggestion [13] that the hydrogen incorporates as a complex with some defect, which has to be present for HEDG to take place. This hydrogen then interacts with the line to alter the saddle point of their migration barrier. This hydrogen-complex would be unstable above 500 °C, however the nature of this defect is unclear. This would be similar to the effect proposed for H-enhanced oxygen diffusion in silicon [14].

A variety of defect structures are possible at a reconstructed dislocation core, notably 'kinks' which are atomic scale steps in the dislocation line between one Peierls valley and the next, and 'solitons' or anti-phase defects, local dangling bond sites that lie at the interface between two sections of dislocation line which have undergone bond reconstruction in different directions. These defects are discussed further in our previous work [2]. Hydrogen is able to complex with both these defect species as well as with the reconstructed Si–Si bonds along the dislocation core.

The lowered prefactor, at higher hydrogen concentration, is thought to arise from the low mean-free path of non H-soliton kink complexes under a substantial flux of H atoms. One possible explanation for HEDG is that if the introduction of hydrogen causes a reduction in the soliton formation energy, soliton density would increase [15]. As a result, the formation rate of kink pairs would increase and thus also dislocation velocity. This suggestion is supported by the fact that the HEDG effect only occurs in elemental semiconductors (Si, Ge), and is absent for α-dislocations in GaAs. Within this context, this would be due to the lack of solitons along α-dislocations as GaAs only weakly reconstructs [12,13].

As mentioned in the introduction the smart-cut process also has a 1.2 eV activation energy within a hydrogen implanted silicon system, suggesting that dislocations may control this process as well. This is further supported by the observation that the smart-cut process does not always lead to a clean separation on one plane; instead it can lead to blisters forming. This is avoided by leaving a *thick* slab of silicon on top. Again this seems to fit dislocation theory and not other explanations provided, for example z-direction Ostwald ripening [16,17]. If the hydrogenated stacking fault region can separate due to the proximity of the crystal surface and thus release its strain, then it can bubble and take on H_2 molecules. If this z-direction expansion is constrained due to thicker material then it is forced to remain as a hydrogenated dislocation [18,19].

Hence we can suggest why the barrier to smart cut is 1.2 eV (hydrogen enhanced dislocation motion) and why the smart cut process is harder in GaAs with its lack of dislocation core reconstruction.

3 The nkMC model

We take on board the idea of multi-scale modelling. Since the computational cost to model an entire dislocation line system at an ab initio level is too high, we use local energy calculations for localized structures and then use these to generate parameters for a large scale algorithmic model.

As in our previous work on silicon dislocation dynamics [1,2], the evolution of the line is achieved via an n-fold way kinetic Monte Carlo [nkMC] [20–24], sometimes called the fast kinetic Monte Carlo[fkMC] [22]. This is parameterized using data previously calculated [11,12], and some new calculations described later.

Dislocation segments are assumed to lie in Peierls minima. The lattice in our nkMC simulations has infinite extent in the direction of motion, whilst periodic perpendicular to it we simulate a dislocation line 1000 re-construction bonds long with periodic boundary conditions. The line moves due to the effects of thermal fluctuation and an

Table 1. Defect structures and their migration barriers used in nkMC simulations.

Defect	Width	Migration Barrier/eV	Source
kink step up/down	0	1.75	Öberg et al. [12]
kink-soliton complex	0	0.29	Ewels et al. [11]
soliton	1	0.15	Ewels et al. [11]
hydrogenated soliton	1	1.05	Ewels et al. [11]
2H in a reconstruction bond (H_{2BC})	1	∞	assumption
Kink-H soliton complex	0	1.16	Ewels et al. [11]
Bond Centred Hydrogen (H_{BC})	1	0.295	new calculation
kink-H_{BC} complex	0	1.16	assumption
			=Kink-H soliton complex
kink-H_{2BC} complex	0	∞	assumption

applied stress. The initial state of the line in all cases is taken to be the perfectly straight single period reconstruction [25,26]. There is also a suggested double period reconstruction [27] for the lowest energy state of the line. However, as the structure will break up as the line moves, our initial choice of starting state should not greatly affect the overall conclusions.

In nkMC [20,21], each event i has a rate r_i calculated for it,

$$r_i = \omega_0 \exp(-\Delta E_i / k_B T) \tag{3}$$

where ΔE_i = the energy barrier of event i and ω_0 = the attempt frequency, for which in most cases we use the silicon Debye frequency [28] $\approx 1.56 \times 10^{13}$ Hz. These rates act as probabilities, and their sum determines the time until the next event.

Instead of trying random events at each time step and accepting them based on a Boltzmann-like criterion, e.g. the Metropolis algorithm [29], we carry out an event m from all the events M at each MC step, such that

$$\frac{\sum_{i=0}^{m-1} r_i}{\sum_{i=0}^{M} r_i} < \xi_1 < \frac{\sum_{i=0}^{m} r_i}{\sum_{i=0}^{M} r_i} \tag{4}$$

where ξ_1 is a random number in the range (0, 1). The time increment dt, for each Monte Carlo [MC] step is dynamic and stochastic, and given by

$$dt = -\frac{\ln \xi_2}{\sum_{i=0}^{M} r_i} \tag{5}$$

where ξ_2 is a second random number in the range (0, 1).

In the standard description of a dislocation line in an MC simulation [30,31], the line is a fixed number of sites long. Each site i has a height H_i associated with it, giving the distance travelled by the dislocation line at that site under the stress. Changes in height between neighbouring sites are assumed to indicate a kink between them. We call this the point-wise description.

Meanwhile, Line-wise is our more flexible description [1,2], and is similar to that of Cai et al. [32,33], in that the line is now described by a variable number of sections. Each section j is described by its length L_j reconstruction bonds and height H_j. However, we also state which defect structure the section ends with E_j, i.e. a positive or negative kink, soliton, etc. A fuller description and the gains in efficiency of line-wise can be found in our previous work [2].

At a high population of defect structures, the distinction between defects located at reconstructed bond sites along the dislocation core and those lying between such sites becomes more important. This is incorporated in the simulations by defining a width for each defect. Kinks and other inter-reconstruction bond defects are width zero, and must keep at least one reconstruction bond apart from other zero width defects. Solitons and other defects that take up a reconstructed bond or bonds are of width one or more, and may abut other defects. A list of all defects used, their migration barriers and their widths can be found in Table 1.

Our description of our model is perhaps slightly misleading here. Strictly speaking our kinks are not zero width, they just do not use up a reconstruction bond along the line. Their width is defined by the atomic structures output from the DFT calculation [11]. From the DFT calculations we can see that the presence of a kink has a minor modification on the silicon bond lengths and angles in neighbouring sites. However such distortions are small, and we have not incorporated them in the Monte Carlo simulation. To do so we would need to include an additional set of moves associated with all possible defects in these kink-neighbour sites, which would lead to an explosion in the range of possible moves. In the case of finite width kinks for other dislocation types, where the kink takes multiple sites along the line, this could be implemented in our model with kink defects with widths greater than 1; however this would lead to an even further increase in the number of different move types to be incorporated and would quickly become impractical. It can be seen that this method of point kink structures along the line is clearly not be applicable for handling delocalized kinks with no clearly defined localised atomic structure, as seen in low Peierls stress materials such as for example copper.

The applied stress is implemented via a bias on the activation energies $\Delta E_i \rightarrow \Delta E_i \pm s$ depending on whether the line is moved with or against the stress, where

$$s = \sigma b l h \tag{6}$$

and σ = applied stress, b = magnitude of Burgers vector of the dislocation, l = length of section moving (i.e. dislocation line repeat distance) and h = height change.

This gives an $s \approx 0.013$ eV for a stress of 70 MPa acting on the 90° partial dislocation in silicon. So as to approximately match the work of Yamashita [8], we have taken this as the applied stress in all the simulations in this work.

To clarify this bias, if a kink step up moved to the right its migration barrier (as stated in Tab. 1) would be decreased by s, as it would move a section of line forward with the stress, whilst if it moved to the left it would have a barrier of $1.75 + s$, as it would be moving a section of line back against the applied stress. Commensurately, the creation of a kink step up-kink step down pair would have its barrier decreased by s, whilst a kink step down-kink step up pair would have its barrier increased.

3.1 The moves from defects on the line

A *move* in a Monte Carlo sense is an event that can take place within the simulation. In this section we describe the process by which we built up the moves implemented in our nkMC simulations, from the defect structures included. These are in addition to the migration moves shown in Table 1.

The first defect structures needed to model dislocation glide are a kink step up and a kink step down. A dislocation line does not move forward in a single step, but instead by the thermally activated process of throwing forward line segments, generating a kink step up and step down pair. These are then forced apart by an external applied stress, and so the dislocation moves into the next Peierls valley.

There is much evidence for the existence of such kinks from pulse deformation, internal friction [34], weak-beam electron microscopy, and spectroscopy [35,36]. This leads to the moves in Section a of Table 2, barriers for which are taken from the calculations of Öberg et al. [12], although quoted here to higher accuracy.

Next, we add solitons. This concept was first proposed by Hirsch [25]; the nomenclature is not universal and other names such as *phase-switching defects*, *anti-phase defects* and *flips* are also used. Depending on its reconstruction a 90° partial core has two phases, depending on which direction the reconstruction bonds form. At phase interfaces, there are anti-phase defects [37] which we refer to here as solitons [15] with a 1.4 eV formation energy. The soliton is an under-coordinated silicon atom, a free-radical in chemical nomenclature, and hence highly reactive and able to migrate rapidly along the line as their migration barrier is only 0.15 eV. The dangling bond of the soliton can catalyze kink formation, and so greatly reduces its energy barrier.

Solitons are incorporated through three additional defect structures: soliton-kink step up complex, soliton-kink step down complex and the soliton itself.

We take further calculations [11] to parameterize the soliton moves, shown in Section b of Table 2, as well as moves that allow kinks to move into/out of solitons and vice-versa, producing/splitting kink-soliton complexes. We assume no binding energy between solitons and kinks. This means that they can pass through each other or move together, using the migration barrier of the moving part of the defect complex.

In our previous work [2], upon addition of solitons we saw a minimal change in system behaviour. However when we fixed their population at an elevated level, they greatly affected line motion, even without a kink-soliton binding energy. This is because although the formation energy (F_k) of a soliton is a thermally accessible 1.4 eV, they are created in pairs due to topological constraints. The time averaged concentrations of the solitons and kink-soliton complexes in these simulations were infinitesimal. They only appeared fleetingly and then were rapidly annihilated, being unable to maintain their thermal equilibrium concentration within the time frame of the simulation.

It is clear then that some process is required to either decrease the activation energy for the formation of solitons or prevent them from annihilating, if they are to play an important rôle in dislocation motion. In HEDG, solitons may become more important, as hydrogen could lower the formation energy of a soliton pair, and also obstruct annihilation by saturating one of the solitons.

We next add hydrogenated solitons (H_{sol}) and hydrogenated soliton-kink step up/down complexes, i.e. soliton defects with their dangling bonds pacified by hydrogen. These are taken from the calculations of Ewels et al. [11], given in Section c of Table 2.

In addition to these moves there are also those for the annihilation of kink pairs. These are taken to be equivalent to the migration of the individual components, as we do not consider any kink-kink repulsion. If one of the kinks are complexed, the item it is complexed with will remain. We also allow for the creation of a H_{2BC}-defect (two hydrogen atoms in the same reconstruction bond), which occurs when a hydrogen containing defect runs into another.

3.2 Hydrogen arrival at the dislocation line

Bond centred hydrogen (H_{BC}) in bulk silicon dilates the Si–Si bond and hence atomic hydrogen will preferentially sit in the dilated reconstruction bonds at the dislocation core. H_2 lies at the tetrahedral interstitial site in bulk Si, and will preferentially sit in the large channel of the dislocation core. In general, both H_2 and atomic hydrogen should be caught in the long-range strain field of the dislocation.

In addition H_2 can in principle occupy a Si–Si bond centre and dissociate to form a pair of Si–H bonds. In bulk silicon this is unstable with respect to molecular H_2 in interstitial voids, since the Si–H..H–Si bonding either causes massive expansion along the Si–Si bond direction or else lattice shear to displace the pair of Si–H bonds. This lattice shear occurs naturally at the core of the 90° partial dislocations in silicon and hence the binding energy of a H_2 molecule to a reconstructed Si–Si bond in the 90° partial core will be more energetically favourable than in the bulk.

The rates for moves due to the influx of hydrogen species on to the dislocation line were constructed using

Table 2. Selection of moves from the HEDG nkMC model.

Section	Move description	Barrier eV	Source
a	creation of a kink pair $=2F_K + W_M$	1.92	Öberg et al. [12]
	annihilation of a kink pair $=W_M$	1.75	Öberg et al. [12]
b	formation of a kink pair at a soliton	0.29	Ewels et al. [11]
	destruction of a kink pair at a soliton	0.18	Ewels et al. [11]
	creation of a soliton pair	2.95	Ewels et al. [11]
	annihilation of a soliton pair	0.15	Ewels et al. [11]
c	formation of a kink pair at a H-soliton	1.16	Ewels et al. [11]
	destruction of a kink pair at a H-soliton	1.35	Ewels et al. [11]
	formation of a H_{2BC} defect from 2 H-solitons	0.29	Ewels et al. [11]
d	expulsion of H_2 (removal of H_{2BC} defect)	0.96	Ewels et al. [11]
e	creation of a kink pair at H_{BC}	1.16	assumption
	destruction of a kink pair at H_{BC}	1.38	new
	H-soliton splits to soliton & H_{BC}	2.344/1.444	new
	H_{2BC} to $2H_{BC}$	0.845	new
	H_{BC} to soliton (expulsion of H)	1.986	new
	H_{2BC} to H_{BC} (expulsion of H)	2.1	new

two standard equations from kinetic theory,

$$\text{flux density} = n\frac{\bar{\nu}}{4} \quad \text{and} \quad \bar{\nu} = \frac{3D}{\lambda} \tag{7}$$

where n = number density, $\bar{\nu}$ = average velocity, D = diffusion coefficient and λ = hydrogen species mean free path within silicon. If we assume that all of the hydrogen species passing within one mean free path of the line are caught, then it can be shown that the rate of H arrival at a given site along the line is given by

$$r_H = \frac{3\pi}{2} nLD \tag{8}$$

where L is the width of a site. This equation makes the zeroth order assumption of a cylindrically symmetric stress field about the dislocation line. Although the physical stress field is more complicated, differences in H flux rate at the line will be reflected in a shift of the temperature regime; this is discussed further below.

We take $D = 5 \times 10^{-7} \exp(-0.48/k_BT)$ ms^{-1}, for atomic hydrogen in crystalline silicon (c-Si) [38–41]. The 0.48 eV migration barrier comes from permeation experiments of Van Wieringen and Warmoltz [38]. These show that for temperatures ≈1000 K the diffusion coefficient has an Arrhenius law form.

There have been some queries about the validity of extrapolating the value for D down to and below room temperature [42,43]. However, in the simulations of this work we will be using temperatures between 500 K and 1000 K and quantum mechanical tunnelling effects are only thought to become important below this range [44–48]. This is supported by the work of Langpape et al. [49] showing that hydrogen diffusion in c-Si undergoes a sharp change in behaviour from $D \propto T^n$, with $n = .56 \pm 0.3$ to $D \propto \exp(-0.48/k_BT)$ at about 200 K, i.e. from a quantum tunnelling diffusion regime to a thermally activated one.

Upon striking the line, we have the hydrogen atom transform into a bond centred hydrogen defect. We also include a soliton being struck and becoming hydrogenated. These moves are equivalent, as we assume that the incoming hydrogen is stabilized by its new surroundings in each case, the only barrier to motion being that already described in D.

We also ran simulations which assumed that the mobile hydrogen species in bulk Si is the hydrogen molecule. For H_2 (neutral) the barrier to diffusion becomes [50] 0.73 eV, this being the barrier to motion of the molecule between interstitial sites. This is close to the experimental value [56] of 0.78 eV. Thus in the H_2 case, $D = 5 \times 10^{-7} \exp(-0.73/k_BT)$. On arrival at the line, the molecule becomes a H_{2BC}-defect.

For interaction of H_{BC} with H_{sol} we have allowed for two cases. Since they can pass through each other with a barrier the same as, or less than, H_{BC} migration along the line, we allow them to exchange places with the H_{BC} migration barrier. Alternatively, although energetically unlikely, we have also included a second possible interaction

$$\mathrm{H_{BC}} + \mathrm{H_{sol}} \rightarrow \mathrm{H_{2BC}} + \text{soliton}. \tag{9}$$

To clarify, in our nkMC simulations we therefore include H arriving at the line as a move that spontaneously creates a H_{BC} defect or replaces a soliton with a hydrogenated soliton with the rate r_H as given by equation (8) and $D = 5 \times 10^{-7} \exp(-0.48/k_BT)$. Whilst, inclusion of H_2 is by a single move that creates a H_{2BC} defect, once again with a rate given by equation 8 but now with $D = 5 \times 10^{-7} \exp(-0.73/k_BT)$.

In each case we vary the relative concentration of the mobile hydrogen species by varying n (number density) in equation (8).

3.3 Hydrogen expulsion from the dislocation line

It has been shown that certain point defects in silicon can act as recombination sites for hydrogen atoms, producing H_2 molecules [65]. This occurs for dopant atoms which trap multiple H atoms, concentrating them together and allowing them to re-bond. However, other point defects (e.g. vacancies and interstitials) can act as dissociation sites for H_2, essentially as part of the passivation of their dangling bonds [66].

In the case of the dislocation line, we have an extended and moving defect with a long range $(1/r)$ strain field which draws in hydrogen species. Once at the line, the H in general remains bound, and is geometrically restricted to one dimension (motion along the line). This massively increases the chances of H recombination, with recombined H_2 molecules able to pipe diffuse away along the dislocation core.

This is implemented in our model by allowing defects containing hydrogen to coalesce and form Si–H–H–Si (the H_{2BC} defect) followed by

$$\mathrm{Si-H-H-Si} \rightarrow \mathrm{Si-Si} \; + \; \mathrm{H_2}. \tag{10}$$

A first approximation to the barrier for this expulsion is 1.70 eV, this being the difference between the formation energies of a H_{2BC}-defect and a H_2 molecule in a dislocation core 7-fold ring.

However, in going from a point like defect to a freely moving molecule (if confined to 1-D) we need to address more fully the free energy of the H_2 species since there will be a significant increase in entropy.

Allowing for translational and rotational freedom of the H_2 gives us for an ideal gas flowing in 1-D,

$$S = \frac{3}{2} k_B \ln T. \tag{11}$$

Assuming that the gas phase entropy of the molecule is much greater than the entropy of H_{2BC} then the change in free energy for H_2 expulsion from the line is now given by

$$\Delta G = \Delta H - \frac{3}{2} k_B T \ln T \tag{12}$$

with $\Delta H = 1.696$ eV. It is this ΔG we use in our simulations as the full barrier to H_2 expulsion.

In vibrational terms we are essentially going from two Si–H vibrations to a Si–Si lattice vibration and a interstitial H_2 molecular vibration. Si–H vibrations are typically around 1900–2200 cm^{-1} in hydrogenated vacancies, platelets and surfaces, which should be locally similar to our H_{2BC} case. This gives us an energy of around 4000 cm^{-1} in the first case, whilst in the second case the Debye frequency of Silicon gives us $\sim$519 cm^{-1} and the interstitial H_2 molecule in silicon [51] is 3618.4 cm^{-1}, a total of $\sim$4100 cm^{-1}. Hence, the entropy of vibration between the two cases, at least to a first approximation, can be said to be equal.

We assume here that once the hydrogen is in a molecular form in the dislocation core it rapidly pipe diffuses out of the system [11], and can therefore be removed from the calculation. These moves are given in Section d of Table 2.

4 Assumptions

Addition of H_{BC} and H_{2BC} to the system adds a vast range of new defect species, barriers and interactions to the system. It is impractical to determine them all at an ab initio level, so we have therefore made a number of assumptions:

1. kink formation at H_{BC} has the same barrier as that of kink formation at a hydrogenated soliton;
2. a kink containing H_{BC} migrates with the same barrier as a kink containing a hydrogenated soliton;
3. H_{BC} binds as strongly to a kink as it does to the main dislocation line;
4. H_{BC}-soliton interaction energies will be the same in a kink as on the line;
5. H_{2BC} is mobile through the formation and subsequent combination of neighbouring H_{BC} (0.54 eV), i.e. $H_{2BC} \rightarrow 2H_{BC} \rightarrow H_{2BC}$;
6. H_{2BC} can only interact with a neighbouring kink via the same H_{2BC} break-up mechanism — i.e. they cannot pass through each other as whole entities, or merge in a single step to form a H_{2BC} at a kink. Thus in effect H_{2BC} will act as a block to any passing kinks. Kinks can however become doubly hydrogenated, by picking up two H_{BC} species.

Although the energies may not be precisely identical in the cases grouped together above, where we have grouped similar move-types together our reasoning is that they involve similar processes and thus will have similar migration barriers. For example in the first assumption, both processes involve a Si–Si bond breaking and formation in the centre step of motion, and thus would be expected to have similar migration barriers. Different hydrogen motion steps are also involved, but our calculated hydrogen migration barriers are significantly lower than the barrier for hydrogenated-soliton kink motion (see below) and so will not be the rate determining step for any hydrogenated-kink motion. Likewise for binding energies, we have grouped together defect types where the local bonding environment for the hydrogen and silicon is similar to that for a case which we have explicitly calculated.

Finally, we note that we have not incorporated the effect of charging on the dislocation line. Charge transfer between isolated solitons and dopants in the bulk may be possible, and may also modify defect formation energies,

for example the energy to create a soliton - hydrogenated soliton pair from H_{BC} at the dislocation core. Notably in bulk Si, isolated H atoms are stable at the bond centred site in the neutral and positive charge states, but as H^- they switch to the anti-bonding or tetrahedral sites.

The various values outlined above were used to parameterize many moves in the nkMC, of which a selection are shown in Section e of Table 2.

5 Density functional method

In order to model hydrogen related defects in the dislocation core at ab initio level we use AIMPRO [52], a density functional code operating under the local spin density approximation. Norm-conserving pseudo-potentials of Bachelet et al. [53] are used. The system is modelled with a 290 atom hydrogen terminated Si cluster $Si_{168}H_{122}$ containing a 90° partial dislocation core and either H or H_2 in various configurations.

A real-space basis is used, with 16 Gaussians per silicon atom (4 each of s-, p_x-, p_y- and p_z-symmetry) and 9 per hydrogen atom to model the molecular wave-functions; 5 s-type Gaussians were used for the valence charge density per silicon and 2 per hydrogen (basis set tests have previously been conducted for these systems [11]). The structure is fully geometrically optimised, i.e. the self-consistent energy E and the force on each atom were calculated and the atoms moved by a conjugate gradient algorithm until structural equilibrium was attained. Full geometric optimisation is necessary in order to obtain accurate defect formation energies, since the strain associated with hydrogen insertion causes significant lattice relaxation in the surrounding material.

Defect formation energies are calculated by adding and subtracting appropriate cluster energies, so for example, the formation of a bond-centred H_2 defect in the dislocation core from two bond-centred H atoms is determined from

$$\Delta H = E(\mathrm{C} - \mathrm{H}_2) + E(\mathrm{C}) - 2E(\mathrm{C} - \mathrm{H}) \qquad (13)$$

where $E(\mathrm{C})$ is the total energy of the base silicon cluster, $E(\mathrm{C} - \mathrm{H})$ total energy of the cluster containing H at the dislocation core, etc.

6 Density functional results

Our previous work focused on the interaction of H with solitons in the dislocation line [11] however it is also possible for H to sit in a bond centred site between two Si atoms (H_{BC}). This is the stable site for H(neutral) and H(+) in bulk silicon and causes a dilation of the Si–Si bond by around 40%. Hence it is likely that H_{BC} will be more stable at a dislocation core where the reconstructed Si–Si bonds are already dilated by 3% and easily able to expand. Indeed we find that H_{BC} binds to the line with an energy of 1.07 eV compared to H_{BC} in the bulk. In this case H_{BC} sits slightly off the bond-centre (Si–H–Si bond angle of 166°) with Si–H distances of 1.69 Å and Si–Si distance of 3.35 Å. A schematic of the H_{BC} defect in the dislocation core can be seen in Figure 1.

H_2 is unstable in a bond-centre in bulk Si due to the lattice compression it exerts. Instead, one H atom moves to an anti-bonding site forming the H_2^* defect. In principle H_2 could adopt a bond-centred site if accompanied with a shear orthogonal to the Si–Si bond, and this is exactly the situation in the 90° partial dislocation core. Thus unlike in bulk, Si bond-centred H_2 at a 90° partial dislocation core (H_{2BC}) is stable. Two isolated H_{BC} atoms in bulk release 2.70 eV when forming H_{2BC} at the dislocation, while two H_{BC} defects already in the dislocation core can combine to H_{2BC} releasing 0.56 eV. Note that if they do so there is a higher energetic cost to separation; two H_{BC} atoms with one Si–Si bond separating them are 0.76 eV less stable than H_{2BC}, since the intervening Si–Si bond is dilated due to surrounding strain. A schematic of the H_{2BC} defect in the dislocation core can be seen in Figure 2.

These new defect species can also interact strongly with soliton defects in the dislocation core, since these are Si dangling bond defects which the hydrogen can saturate. Our previous calculations showed that H_{BC} in the bulk binds to a soliton in the core with a binding energy [11] of 2.56 eV. These new calculations show that H_{BC} in the dislocation core will also bind to a bare soliton to form a hydrogenated soliton (H_{sol}), releasing 1.51 eV. A schematic of the H_{sol} defect in the dislocation core can be seen in Figure 3.

Part of the reason solitons do not appear to affect non-hydrogenated dislocation motion [2] is the high energetic cost of splitting a Si–Si bond at the dislocation core into two solitons (2.8 eV [11]). H_{BC} in the dislocation core can split into a pair of solitons, one hydrogenated, the other not. This requires only 1.29 eV, i.e. less than half that of normal soliton pair formation. Thus bond-centred H can catalyze soliton formation. However H_{2BC} will not form unhydrogenated solitons; indeed it can act as a sink for unhydrogenated solitons, via the reaction

$$\mathrm{H}_{2BC} + \text{soliton} \rightarrow \mathrm{H}_{BC} + \mathrm{H}_{sol}$$
$$\Delta H = -0.95\,\mathrm{eV}. \qquad (14)$$

Thus we might expect at low [H] H_{BC} will catalyze the production of solitons, whereas at higher [H], H_{2BC} will act as a soliton 'sink'. This transition is discussed further in the context of the nkMC results.

We have calculated the migration barrier for H_{BC} along the dislocation line. The H atom moves by breaking one Si–H bond and forming the next, while maintaining a shared Si–H bond through this motion. Since the motion therefore requires the breaking of a single bond and the formation of another, we can trace the diffusion profile by restricting the ratio of these two bond lengths r_1 and r_2 such that

$$r_1^2 - r_2^2 = c_1 \qquad (15)$$

where c_1 is a constant. By relaxing the system with different values of c_1 we obtain a diffusion profile. All other

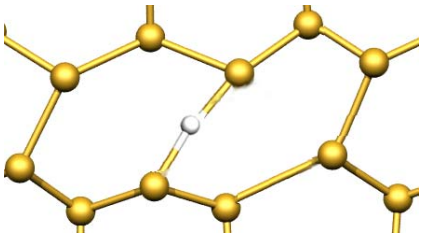

Fig. 1. Schematic showing a bond centred hydrogen defect (H_{BC}) in the core of a 90° partial dislocation core in silicon. The dislocation line runs from left to right and moves in the plane of the paper; the angled diagonal bonds are reconstructed Si–Si bonds lying along the dislocation core.

Fig. 2. Schematic of the H_{2BC} defect (i.e. two hydrogen atoms in the same bond centre) in the core of a 90° partial dislocation in silicon.

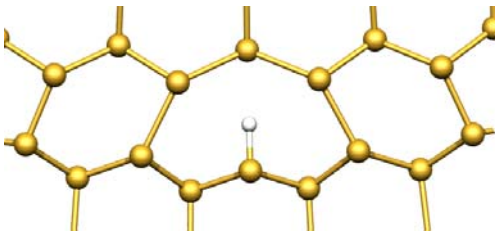

Fig. 3. Hydrogenated soliton defect in the dislocation core.

atoms are allowed to geometrically relax with no constraint. This reaches the mid-point of motion, bringing the H_{BC} to a reconstructed Si–Si bond centre of the opposite sign to those around it. A symmetrically equivalent diffusion then moves it into the next reconstructed Si–Si bond centre of the correct sign.

These calculations give the migration barrier for H_{BC} along the dislocation line to be 0.295 eV. This is consistent with calculations for H_{BC} in the bulk [54], where H^+ was found to migrate with a barrier of ∼0.2 eV, and experimental bulk H^+ measurements which give a value [55] of 0.43 eV. We note that H diffusion barriers calculated using LSDA are often lower than those given using GGA by the order of ∼10%. For example calculations of H diffusion on Si (001) surfaces give a barrier of 1.39 eV using LDA and 1.55 eV with GGA (compared to 1.68 eV from experiment) [57].

7 Line-wise nkMC results

In the nkMC simulations described here, run lengths of ten million MC steps were used. As stated before the system simulated was 1000 reconstruction bonds wide, biased with an applied stress of 70 MPa, also the temperature T was varied between 500 and 1000 K, in steps of 100 K.

Although highly studied, diffusion of hydrogen through silicon is still not well understood. This is partly as it diffuses as multiple forms: neutral H^0, charged (H^+, H^-) or as the molecule H_2. H_2 gas heated with silicon enters as atomic hydrogen. The high activation energy of 3.6 eV for the elimination of hydrogen from silicon at 500 °C also suggests atomic hydrogen.

Although we accept that hydrogen most likely exists in bulk Si as a mixture [58] of both H and H_2, we initially model each separately, starting with neutral atomic hydrogen striking the line. H atom concentration n, was varied as 10^m cm^{-3}, in steps of m from 1 to 20.

Figure 4 shows contour plots of average concentration of each defect component against temperature (K) and m.

Note that the concentrations are per reconstruction bond and are quoted for the components of each defect. Thus, for example, a hydrogenated soliton-kink complex will contribute both to the concentration of kinks and of hydrogenated solitons. The H_{2BC} defect has width one, whereas the H_{2BC}-kink complex has width zero. This means that the concentration of H_{2BC} can reach a theoretical maximum of two, since in the case of an alternating series of H_{2BC}-kink complexes and H_{2BC} defects, there will be $2H_{2BC}$ per reconstruction bond. For clarity however we have rescaled the plots to run in all cases from concentrations of 0 (no presence) to 1 (maximum possible density for that species).

We also show rate of H_2 expulsion, see Figure 5a.

Unfortunately, a common problem for MC simulations is that nature rarely takes place on one time-scale. In the system that we are investigating, the time-scale of the interaction of the defects along the line is far faster than the time-scale of motion of the line itself. This means that our nkMC may automatically concentrate on the defect interactions in certain regimes. This coupled with the variable time-step of the nkMC means that for a given number of MC steps, the nkMC may simulate a different length of time depending on the temperature and influx of hydrogen. This can vary by orders of magnitude, which must be taken into account in any analysis, and so a plot of log(simulated time duration) is included in Figure 5b.

Essentially, if we reach a state were most of the possibly moves have low rates then equation (5) (which determines the simulation time-step) will on average give a longer step. Alternatively, in a state were most possibly moves have high rates, then equation (5) gives the reverse result and on average far shorter time-steps.

The identification of molecular hydrogen in silicon has been a major challenge ever since an interstitial species was first proposed by theory [59,60], and more recently it has been shown to be involved in the annealing of the divacancy in silicon [61]. Isolated hydrogen molecules are stable in c-Si [62–64], however only in perfect or near-perfect Si. If the molecule is near stretched, distorted or otherwise weakened Si–Si bonds, it dissociates with a substantial gain in energy. This forms 2 Si–H bonds (our H_{2BC} defect) and a reduction in the strain associated with the

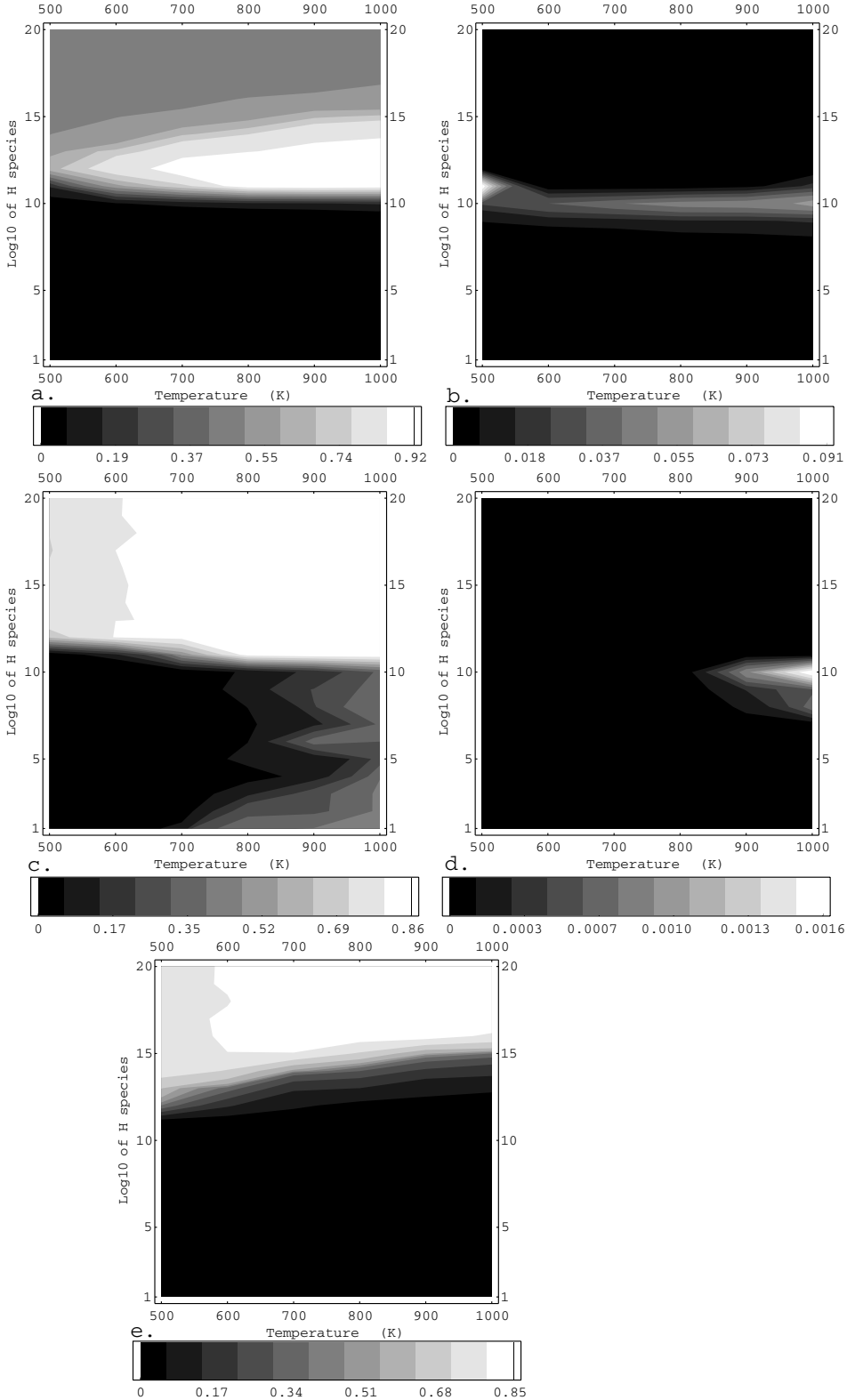

Fig. 4. Results from atomic regime simulations. Concentration of (a) H_{2BC}; (b) bond centred hydrogen; (c) kinks; (d) solitons; (e) hydrogenated solitons.

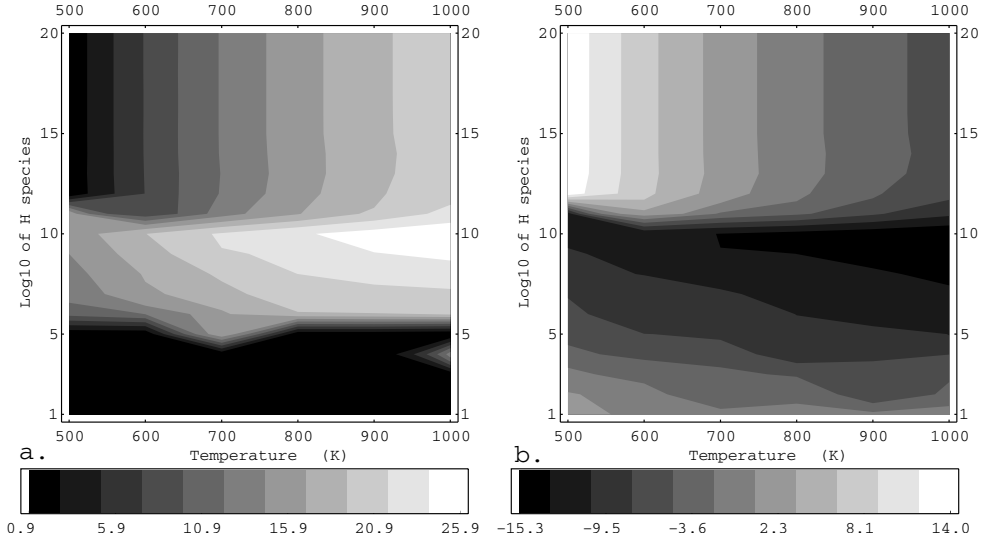

Fig. 5. Results from atomic regime simulations. (a) Log of H_2 expulsion rate; (b) Log of simulated time.

defect. For our second set of simulations we assume an influx of H_2 molecules. The H_2 molecule concentration n, was varied as 10^m cm^{-3} in steps of m from 1 to 20, and upon arriving at the line produced a H_{2BC}-defect.

Plots commensurate with those in Figures 4 and 5 for the molecular regime simulations are shown in Figures 6 and 7.

So as to carry out comparisons with the HEDG experiments we also fitted Arrhenius plots to the final dislocation line velocity in the two hydrogen type regimes for each concentration, allowing determination of effective activation energies E_A and prefactors k. These are shown in Figures 8 and 9, plotted against log of incoming hydrogen species concentration for each regime.

8 Discussion

8.1 Hydrogen enhanced dislocation glide — HEDG

Experimentally, both activation energy and prefactor of the dislocation line velocity decrease when HEDG takes place [8], and indeed our results show both of these drops (see Figs. 8 and 9). Our results even seem to reproduce the experimental activation energy of 1.2 eV, showing ∼1.25 eV in the atomic simulations at a concentration of 10^7 cm^{-3} and ∼1 eV in the molecular simulation at a concentration of 10^5 cm^{-3}. This suggests that if we can assume a linear supposition of these two systems that HEDG is primarily caused by atomic hydrogen striking the line, but with molecular hydrogen lending some assistance.

For there to be an increase in the velocity of the line due to an influx of hydrogen one would at first expect to see a matching increase in a mobile hydrogen containing defect. The two options we have for this are H_{BC} and H_{sol}. However, if we return to the fundamental theories of both Hirth and Loathe [67], Kawata and Ishiota [68], both show that a dislocation line is most likely to move rapidly when a defect essentially affects an empty line and is allowed to move the whole length before encountering a further defect.

Hence the increases in all hydrogen species above and around ∼10^{10} cm^{-3} in the atomic case (shown in Figs. 4a, 4b and 4e) and above and around ∼10^{12} cm^{-3} in the molecular case (shown in Figs. 6a, 6b, 6e) actually suggest that the line is becoming clogged, and is locking up. This is especially true since the H_{2BC} defect is not very mobile, whose increase we see commensurate with an increase in kinks.

Essentially, at these higher hydrogen concentrations, H_2 is occupying all available sites and so restricting the possibility for kink formation. H_2 also blocks kink motion (both by being next to and within a kink) and so will further slow dislocation line motion. This explains the increase in kinks at these conditions. We shall explore these issues in connection with hydrogen recombination in the next section.

Experimentally, HEDG is observed in the temperature regime ∼650–750 K, and is suppressed above around 775 K. We see only a slight increase in the concentration of some defect components as we go to higher temperatures. However, we must bare in mind that at these elevated temperatures hydrogen will be driven from of the sample spontaneously via surface effects and out-diffusion not related to dislocations. This would lead to a shift into low concentration behaviours and so HEDG would indeed stop. Further calculations could in future incorporate this explicitly, via a modification of the H flux reaching the dislocation line including temperature dependent stability of H_{2BC}, H_{BC} and H_2 in the bulk.

The secondary peaks in kink concentration in Figures 4c and 6c at lower hydrogen concentrations are due to a shift in the timescale of the nkMC algorithm mentioned earlier, and shown in Figures 5b and 7b. At lower rates of H addition to the line, the nkMC shifts to longer time scales and starts spontaneously generating kinks as opposed to the shorter timescales observed at higher [H]. If

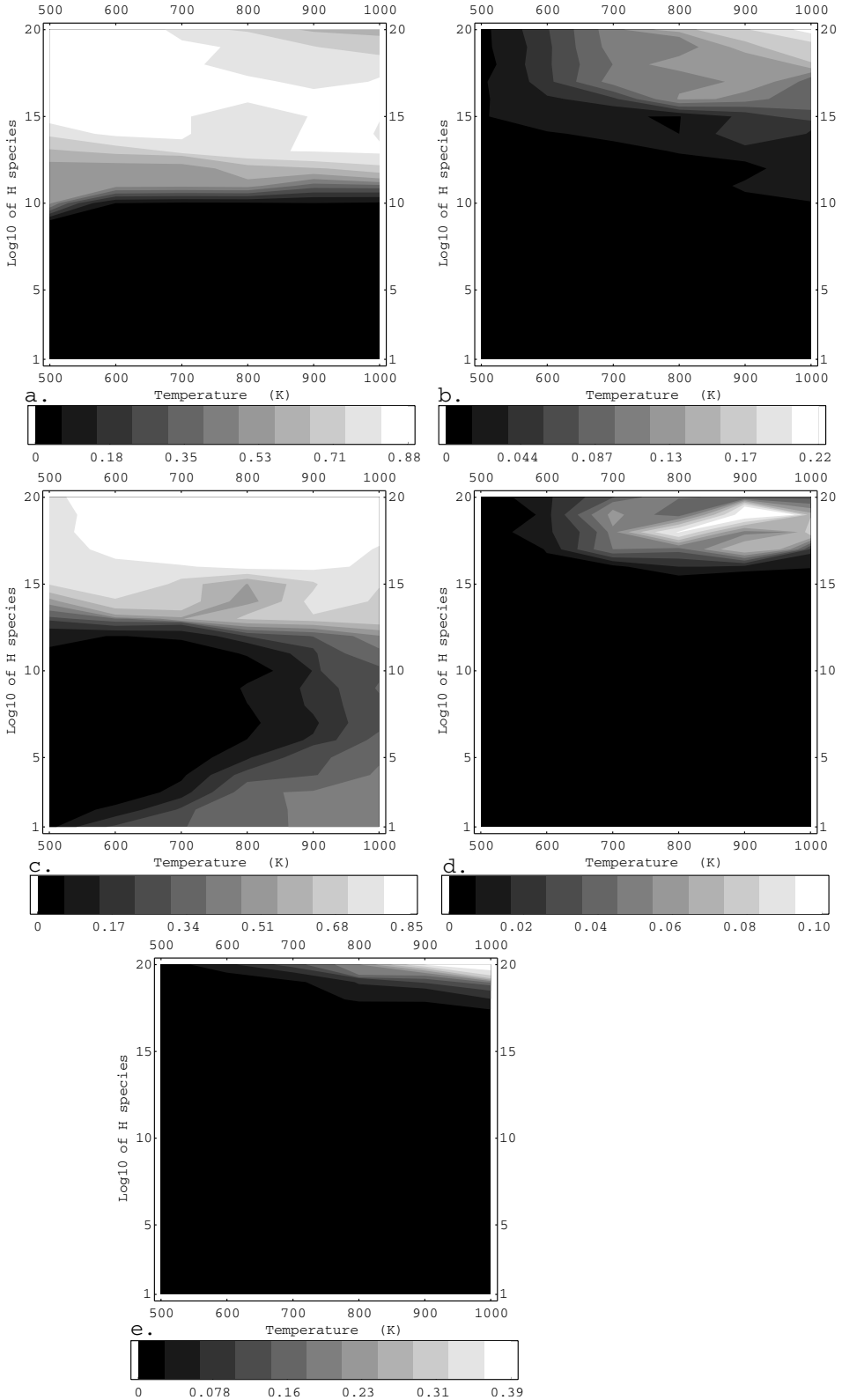

Fig. 6. Results from molecular regime simulations. Concentration of (a) H_{2BC}; (b) bond centred hydrogen; (c) kinks; (d) solitons; (e) hydrogenated solitons.

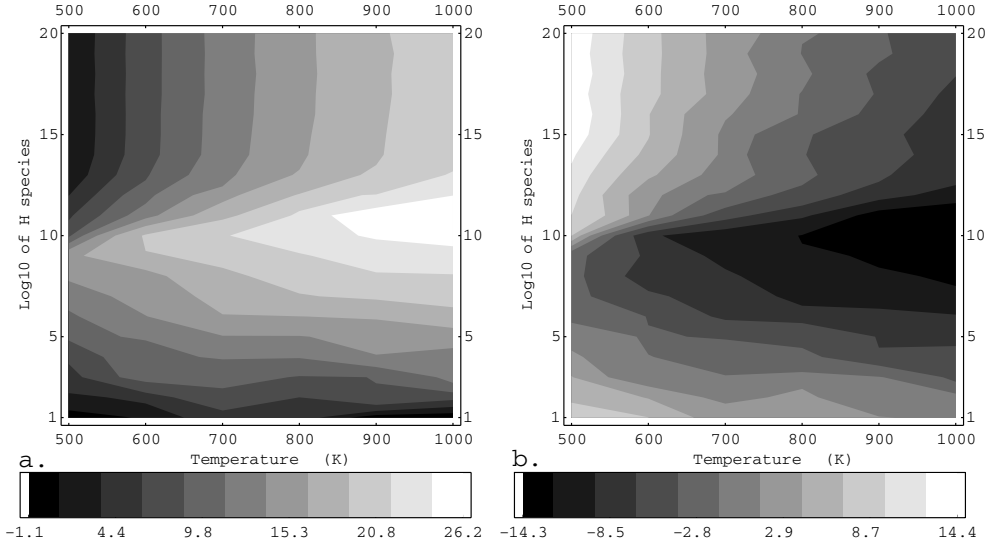

Fig. 7. Results from molecular regime simulations. (a) Log of H_2 expulsion rate; (b) Log of simulated time.

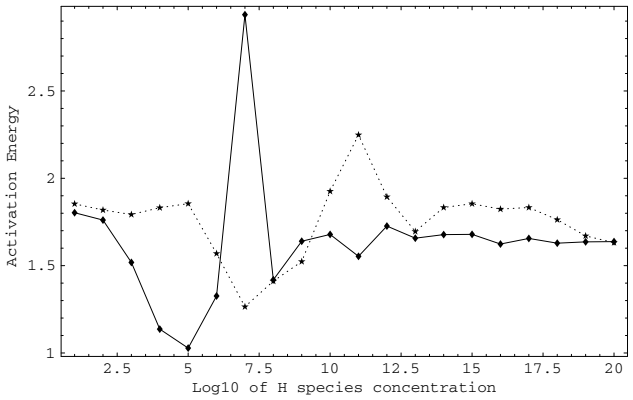

Fig. 8. Plot of activation energy in eV against Log of hydrogen arrival species concentration. Broken line for atomic regime and solid for molecular regime.

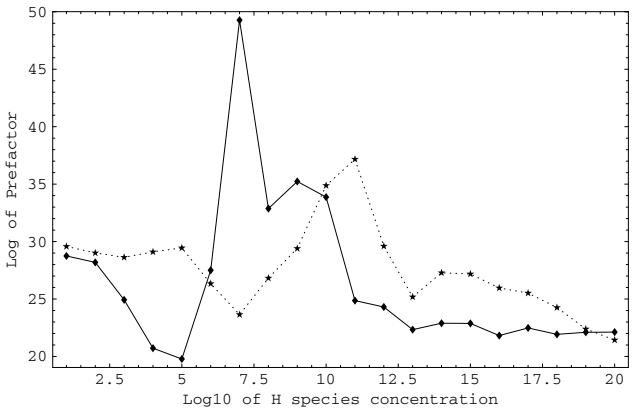

Fig. 9. A log-log plot of prefactor against hydrogen arrival species concentration. Broken line for atomic regime and solid for molecular regime.

it were possible to run fixed time calculations over all [H] these secondary peaks would most likely disappear.

8.2 Hydrogen recombination

If we compare Figure 8 with Figures 5a and 7a, as we go towards the HEDG concentrations in both regimes we see an increase in the rate of H_2 expulsion (and hence hydrogen recombination) as the line becomes easier to move. The expulsion rate then peaks as the line becomes harder to move past the HEDG regime, and then saturates at a lower rate after the activation energy peak.

This suggests that H_2 is given off from the line as a by-product of the HEDG process. Once we get past hydrogen concentrations suitable for HEDG the simulations change focus to concentrate on the hydrogens moving on and off the line with the peak in H_2 expulsion and the large decrease in the amount of time the simulations represent as shown in Figures 5b and 7b, due to a large amount of high rates moves keeping dt in equation (5) low.

After this the simulations suggest that if the incoming hydrogen concentration goes far above the level required for HEDG then further hydrogen arriving at the line slows the progress of the dislocation. This is shown by the elevated H_{2BC} and kink concentrations at [H] above those for HEDG. In addition the time-scale of our simulation begins to increase again as the line becomes clogged with H_{2BC}-defects.

We must also take into account that at ultra-high concentrations, the simulations begin to break down due to a lack of moves that break free from the 1-D constraints of the dislocation, for example moves that lead to platelet formation. This would also lead to a further increase in simulated time, since the simulation with its line completely choked with H_{2BC} defects would have to resort to very high barrier moves, which blocks high rate moves and hence increases dt in equation (5).

What is at first glance surprising is that the atomic hydrogen regime achieves a higher H_{2BC} peak than the molecular one (see Figs. 4a and 6a). However we note that a possible move for an incoming H_2 molecule is to simply move off the line into the dislocation core, whereas atomic H must seek out a partner to achieve this. Coupled with the lower migration barrier for atomic hydrogen approaching the dislocation line, this allows a slightly higher build up of H_{2BC} along the line.

9 Conclusions

Our density functional calculations show that bond centred hydrogen is strongly stabilised in a 90° partial dislocation core in silicon, due the relative dilation of the Si–Si bonds compared to those in the bulk. In addition the offset of the Si–Si bonds at the core allow for stable incorporation of two H atoms into the same Si–Si bond site, producing a canted 'hydrogen bridge' structure.

Our nkMC results suggest that HEDG occurs at H concentrations of around 10^7 cm^{-3} if the dominant H species is atomic, or in the range 10^4–10^5 cm^{-3} for molecular hydrogen. We expect the actual case to be predominately atomic hydrogen with additional support from molecular.

At higher H concentrations the line tends to saturate with hydrogen, leading to higher concentrations of H_{2BC}, kinks and kink-H_{2BC}. This restricts the catalytic formation of new kink pairs, and thus at high [H] dislocation motion is actually impeded. In addition H_{2BC} acts to block kink motion along the line.

Experimentally HEDG is seen in the temperature range ∼650–750 K and suppressed at higher temperatures, which we do not observe. However, at these elevated temperatures H will be driven from the sample, shifting behaviour into lower hydrogen concentration regimes and so stopping HEDG.

As we approach HEDG conditions we show an increasing production rate of H_2 molecules at the dislocation core, and if H in bulk Si occurs as atomic H then under HEDG conditions a dislocation acts as an efficient H recombination site. In effect the dislocation can be seen as a hydrogen powered motor; absorbing atomic H as its fuel from the surrounding lattice which then drives the production and motion of kinks, and expelling H_2 molecules as its exhaust.

We note that fluorine enhanced dislocation glide [FEDG] has also being been proposed [69], many of the basic structures being equivalent to those in the HEDG case. Our method may also be applied to look for an equivalent HEDG effect in diamond [70].

We would like to thank the Sussex High Power Computing Initiative [SHPCI] for the use of the BFG computer system, and Robert 'Bob' Jones and Patrick Briddon the co-creators of the AIMPRO code.

References

1. S. Scarle, N. Martsinovich, C.P. Ewels, M.I. Heggie, Physica B **308–310**, 493 (2001)
2. S. Scarle, C.P. Ewels, M. Martsinovich, M.I. Heggie, Phys. Rev. B **69**, 075209 (2004)
3. N.M. Johnson, C. Herring, D.J. Chadi, Phys. Rev. Lett. **56**, 769 (1986)
4. K. Bergmon, M. Stavola, S.J. Pearton, J. Lopata, Phys. Rev. B **37**, 2776 (1988)
5. A.A. Bonapasta, Phys. Rev. B **46**, 10119 (1992)
6. M. Bruel, Electron. Lett. **31**, 1201 (1995)
7. A.Y. Usenko, W.N. Carr, B. Chen, J. Mater. Sci. Mater. Elec. **14**, 305 (2003)
8. Y. Yamashita, F. Jyobe, Y. Kamiura, K. Maeda, Phys. Status Solidi (a) **171**, 27 (1999); Mater. Sci. Forum **258**, 313 (1997)
9. S.-Y. Tang, K. Gutjahr, S. Hopfe, U. Goesele, Appl. Phys. Lett. **70**, 1390 (1997)
10. S. Pizzini, Phys. Stats. Solidi (a) **171**, 123 (1999)
11. C.P. Ewels, S. Leoni, M.I. Heggie, P. Jemmer, E. Hernádez, Phys. Rev. Lett. **84**, 690 (2000)
12. S. Öberg, P.K. Sitch, R. Jones, M.I. Heggie, Phys. Rev. B **51**, 13138 (1995)
13. K. Maeda, K. Suzuki, Y. Yamashita, Y. Mera, J. Phys. Cond. Matt. **12**, 10079 (2000)
14. R.C. Newman, J.H. Tucker, A.R. Brown, S.A. McQuaid, J. Appl. Phys. **70**, 3061 (1991)
15. M. Heggie, R. Jones, Phil. Mag. B **38**, 365 (1983); **48**, 379 (1983)
16. B. Aspar, H. Moriceau, E. Jalaguier, C. Lagahe, A. Soubie, B. Biasse, A.M. Papon, A. Claverie, J. Grisolia, G. Benassayag, F. Letertre, O. Rayssac, T. Barge, C. Maleville, B. Ghyselen, J. Elec. Mat. **30**, 834 (2001)
17. J. Grisolia, F. Cristiano, B. DeMauduit, G. Ben Assayag, F. Letertre, B. Aspar, L. Di Cioccio, A. Claverie, J. Appl. Phys. **87**, 8415 (2000)
18. N. Martsinovich, M.I. Heggie, C.P. Ewels, P.R. Briddon, Physica B **340**, 654 (2003)
19. N. Martsinovich, M.I. Heggie, C.P. Ewels, J. Phys.: Condens. Matter **15**, 52815 (2003)
20. A.B. Bortz, M.H. Kalos, J.L. Lebowitz, J. Comp. Physiol. **17**, 10 (1975)
21. G.N. Hassold, E.A. Holm, Comput. Phys. **7**, 97 (1993)
22. F.M. Bulnes, V.D. Pereyra, J. L. Riccardo, Phys. Rev. E **58**, 86 (1998)
23. G.H. Gilmer, J. Crystal Growth, **35**, 15 (1976)
24. P.A. Maksyn, Semicond. Sci. Technol. **3**, 594 (1988)
25. P.B. Hirsch, J. Phys. France Colloq. **40**, C6-27 (1979)
26. R. Jones, J. Phys. France **40**, C6-33 (1979)
27. R.W. Nunes, J. Bennetto, D. Vanderbilt, Phys. Rev. B **57**, 10388 (1998)
28. G. Dolling, *Inelastic Scattering of Neutrons in Solids and Liquids* (Chalk River, 1962), Vol. II, pp. 37–48 (1963)
29. N. Metropolis, D.W. Rosenbluth, M.N. Rosenbluth, A.H. Teller, E. Teller, J. Chem. Phys. **21**, 1087 (1953)
30. C.C. Battaile, D.J. Srolovitz, J.E. Butler, J. Appl. Phys. **82**, 6293 (1997)
31. K. Lin, D.C. Chrzan, Phys. Rev. Lett. **60**, 3799 (1999)
32. W. Cai, V.V. Bulatov, J.F. Justo, A.S. Argon, S. Yipp, Phys. Rev. Lett. **84**, 3346 (2000); W. Cai, V.V. Bulatov, J.F. Justo, A.S. Argon, S. Yipp, Comp. Mats. Sci. **23**, 124 (2002)

33. W. Cai, V.V. Bulatov, S. Yip, J. of Comp. Aided Materials Design **6**, 175 (1999)
34. K. Maeda, M. Inoue, K. Suzuki, H. Amasuga, M. Nakamura, E. Kanematsu, J. Physique III, **7**, 145 (1997)
35. J.C.H. Spence, Elec. Mic. Anal. **153**, 23 (1997)
36. W. Benoit, G. Gremaud, B. Queuet, Mat. Sci. Eng. A, **164**, 42 (1993)
37. P.B. Hirsch, J. Phys. **40**, C6-C117 (1979); P.B. Hirsch, J. Microsc. **118**, 3 (1980)
38. A. Van Wieringen, N. Warmholtz, Physics **22**, 849 (1956)
39. C.H. Seager, R.A. Anderson, J.K.G. Panitz, J. Mater. Res. **2**, 96 (1987)
40. C.H. Seager, R.A. Anderson, Appl. Phys. Lett. **53**, 1181 (1988)
41. M. Kemp, H.M. Branz, Phys. Rev. B **47**, 7067 (1993)
42. S.J. Pearton, J.W. Corbett, M. Stavola, *Hydrogen in Crystalline Semiconductors* (Springer-Verlag, Berlin, 1992)
43. S.J. Pearton, Int. J. Mod. Phys. B **8**, 1093 (1994)
44. C.P. Herrero, Phys. Rev. B **55**, 9235 (1997)
45. E.E. Haller, B. Joós, L.M. Falicov, Phys. Rev. B **21**, 4729 (1980)
46. K. Muro, A.J. Sievers, Phys. Rev. Lett. **57**, 897 (1988)
47. E. Artacho, L.M. Falicov, Phys. Rev. B **43**, 12507 (1991)
48. Y.M. Cheng, M. Stavola, Phys. Rev. Lett. **73**, 3419 (1994)
49. Ch. Langpape, S. Fabian, Ch. Klatt, S. Kalbitzer, Appl. Phys. A **64**, 207 (1997)
50. B. Hourahine, R. Jones, S. Öberg, P.R. Briddon, E-MRS meeting (Strasbourg 1998); B. Hourahine, R. Jones, S. Öberg, R.C. Newman, P.R. Briddon, E. Roduner, Phys. Rev. B **57**, R12666 (1998)
51. J.A. Zhou, M. Stavola, Phys. Rev. Lett. **83**, 1351 (1999)
52. P.R. Briddon, R. Jones, Phys. Stat. Solidi B **217**, 131 (2000)
53. G.B. Bachelet, D.R. Hamann, M. Schlüter, Phys. Rev. B **26**, 4199 (1982)
54. C.G. Van de Walle, P.J.H. Denteneer, Y. Bar-Yam, S.T. Pantelides, Phys. Rev. B **39**, 10791 (1989)
55. Y.V. Gorkelkinskii, N.N. Nevinnyi, Mater. Sci. Eng. B **36**, 133 (1996)
56. V.P. Markevich, M. Suezawa, J. Appl. Phys. **83**, 2988 (1998)
57. D.R. Bowler, M. Fearn, C.M. Goringe, A.P. Horsfield, D.G. Pettifor, J. Phys.: Cond. Matt. **10**, 3719 (1998)
58. B.C. Pan, R. Biswas, J. Non-Cryst. Solids **333**, 44 (2004)
59. A. Mainwood, A.M. Stoheham, Physica B, C **116**, 101 (1983)
60. J.W. Corbett, S.N. Sahu, T.S. Shi, C.C. Snyder, Phys. Lett. **93A**, 303 (1983)
61. E.V. Monakhov, A. Ulyashin, G. Alfieri, A.Yu. Kuznetsov, B.S. Avset, B.G. Svensson, Phys. Rev. B **69**, 153202 (2004)
62. K.J. Chang, D.J. Chadi, Phys Rev. B **40**, 11644 (1989)
63. C.G. Van de Walle, Phys. Rev. B **49**, 4579 (1994)
64. S.K. Estreicher, M.A. Roberson, Dj.M. Maric, Phys. Rev. B **50**, 17018 (1994)
65. S.J. Pearton, J.W. Corbett, J.T. Borenstein, *Proceedings of the 6th Triste Semiconductor Symposium*, Trieste, Italy (Ref. 1)
66. S.K. Estreicher, J.C. Hastings, P.A. Fedders, Phys. Rev. B **57**, R12663 (1998)
67. J.P. Hirth, J. Lothe, *Theory of Dislocations*, 2nd edn. (Kriieger, Malabar, Florida, 1982)
68. Y. Kawata, S. Ishiota, Philos. Mag. A **48**, 921 (1983)
69. R. Hull, E.A. Stach, R. Tromp, F. Ross, M. Reuter, Phys. Stat. Sol. a **171**, 133 (1999)
70. S. Jenkins, M.I. Heggie, J. Phys: Cond. Matter **12**, 10325 (2000)